HHS Public Access

Author manuscript

Eur J Pharm Sci. Author manuscript; available in PMC 2024 February 27.

Published in final edited form as:

Eur J Pharm Sci. 2023 April 01; 183: 106370. doi:10.1016/j.ejps.2023.106370.

Lipid nanoparticle-mediated mRNA delivery in lung fibrosis

Matteo Massaro[a,b,†], **Suhong Wu**[a,†], **Gherardo Baudo**[a,b], **Haoran Liu**[a], **Scott Collum**[c], **Hyunho Lee**[a], **Cinzia Stigliano**[d], **Victor Segura-Ibarra**[a], **Harry Karmouty-Quintana**[c], **Elvin Blanco**[a,e,f,*]

[a]Department of Nanomedicine, Houston Methodist Research Institute, Houston, TX 77030 United States

[b]College of Materials Sciences and Opto-Electronic Technology, University of Chinese Academy of Sciences, Beijing 100049 China

[c]Department of Biochemistry and Molecular Biology, Divisions of Critical Care, Pulmonary and Sleep Medicine, Department of Internal Medicine, University of Texas Health Science Center at Houston, Houston, TX 77030, United States

[d]Department of Neurosurgery, Center for Neuroregeneration, Houston Methodist Research Institute, Houston, TX 77030 United States

[e]Department of Cardiology, Houston Methodist DeBakey Heart and Vascular Center, Houston Methodist Hospital, Houston, TX 77030 United States

[f]Department of Medicine, Weill Cornell Medical College, New York, NY 10065, United States

Abstract

mRNA delivery enables the specific synthesis of proteins with therapeutic potential, representing a powerful strategy in diseases lacking efficacious pharmacotherapies. Idiopathic pulmonary fibrosis (IPF) is a chronic lung disease characterized by excessive extracellular matrix (ECM) deposition and subsequent alveolar remodeling. Alveolar epithelial type 2 cells (AEC2) and fibroblasts represent important targets in IPF given their role in initiating and driving aberrant wound healing responses that lead to excessive ECM deposition. Our objective was to examine a lipid nanoparticle (LNP)-based mRNA construct as a viable strategy to target alveolar epithelial cells and fibroblasts in IPF. mRNA-containing LNPs measuring ~34 nm had high encapsulation efficiency, protected mRNA from degradation, and exhibited sustained release kinetics. eGFP

*Corresponding author at: Department of Nanomedicine, Houston Methodist Research Institute, 6670 Bertner St., M.S. R8-116, Houston, TX 77030, United States, eblanco@houstonmethodist.org (E. Blanco).

†Contributed equally

Author contributions

MM designed research studies, conducted experiments, acquired and analysed data, and wrote the manuscript; SW designed research studies, conducted experiments, and acquired and analysed data; GB, HL, SC, HL, CS, and VS-I conducted experiments and acquired and analysed data; HK-Q supervised, designed research studies, and edited the manuscript; EB supervised, designed research studies, and wrote the manuscript.

Declaration of Competing Interest

None

Supplementary materials

Supplementary material associated with this article can be found, in the online version, at doi:10.1016/j.ejps.2023.106370.

mRNA LNP transfection in human primary cells proved dose- and time-dependent *in vitro*. In a bleomycin mouse model of lung fibrosis, luciferase mRNA LNPs administered intratracheally led to site-specific lung accumulation. Importantly, bioluminescence signal was detected in lungs as early as 2 h after delivery, with signal still evident at 48 h. Of note, LNPs were found associated with AEC2 and fibroblasts *in vivo*. Findings highlight the potential for pulmonary delivery of mRNA in IPF, opening therapeutic avenues aimed at halting and potentially reversing disease progression.

Keywords

Lipid nanoparticles (LNPs); mRNA; Idiopathic pulmonary fibrosis; Gene delivery; Alveolar epithelial cells; Lung fibroblasts

1. Introduction

Idiopathic pulmonary fibrosis (IPF) is a progressive, irreversible, and lethal interstitial lung disease (ILD) with an estimated prevalence of 10-60 cases per 100,000 individuals in the US (Lederer and Martinez, 2018). The prognosis of IPF is particularly dismal, with a median survival of 2-5 years upon diagnosis (Sheng et al., 2020), a prognosis comparable to that of metastatic disease in several cancers. Increasing hospitalization rates point towards elevated cases of IPF globally (Hutchinson et al., 2015), warranting effective treatment strategies to combat the disease.

IPF is characterized by extensive extracellular matrix (ECM) deposition in lungs due to an inability to deactivate normal repair processes that respond to repetitive injury to the alveolar epithelium (Chen et al., 2016). Initially considered an inflammatory disease due to the higher number of inflammatory cells in the lungs and eventual progression towards established fibrosis, insights into underlying mechanisms governing IPF progression point towards IPF being an epithelial-driven disease (Selman and Pardo, 2020). Alveolar epithelial type 2 cells (AEC2) in IPF suffer from molecular-level abnormalities that include senescence, dysregulated cell signaling, telomere and mitochondrial dysfunction, apoptosis, and epithelial–mesenchymal transition (EMT) to name a few (Selman and Pardo, 2014). Aberrantly activated epithelial cells in IPF release a variety of factors, including transforming growth factor beta (TGF-β), fibroblast growth factor (FGF), and matrix metalloproteinases (MMPs), in addition to chemokines and cytokines, that lead to fibroblast migration and proliferation (King et al., 2011). These mediators contribute to fibroblast differentiation into myofibroblasts, the latter adopting an apoptosis-resistant phenotype that continuously secretes ECM components (Pedroza et al., 2016). Ultimately, alveolar remodeling and parenchymal fibrosis, in addition to bronchial dilatation, impairs gas exchange, resulting in progressive respiratory insufficiency (Raghu et al., 2011).

Pharmacological treatments have been used in the management of IPF, yet several limitations exist. While the combination of the corticosteroid prednisone, the immunosuppressive azathioprine, and the mucolytic *N*-acetylcysteine was the standard of care for IPF patients, the 2015 American Thoracic Society, European Respiratory Society, Japanese Respiratory Society and Latin American Thoracic Association (ATS/ERS/JRS/

ALAT) international guidelines strongly recommended against the combined use of these due to adverse side effects (Martinez et al., 2017). The 2015 ATS/ERS/JRS/ALAT guidelines did conditionally recommend pirfenidone (Noble et al., 2016 and nintedanib (Richeldi et al., 2011), with both drugs showing physiological benefits in patients. Importantly, while these and treatments such as pulmonary rehabilitation can alleviate symptoms and preserve lung function, there is no effective treatment at present available for IPF patients other than lung transplantation.

An enhanced understanding of IPF initiation and progression have led to the identification of several viable targets that prove ideal for gene therapy. The upregulation or downregulation of gene expression has proven to be quite promising, especially with strategies involving small interfering RNAs (siRNAs, (Davis et al., 2010) and more recently, the use of messenger RNAs (mRNAs) in vaccines against SARS-CoV-2 (Creech et al., 2021). Of note, nanoparticle (NP)-based platforms have emerged as suitable vehicles for gene therapy (Tokatlian and Segura, 2010; Zhao and Huang, 2014; Conley and Naash, 2010). NPs prove more suitable than adenoviral vectors due to their delivery efficiency, ease of manufacture, and ability to bypass the risk of creating a replication competent virus (Douglas, 2007), as well as avoidance of acute inflammatory responses and side effects in immunocompromised individuals (Wang and Zhang, 2021). NPs allow for incorporation of rational design considerations, including moieties for higher cell uptake and rapid endosomal escape (Blanco et al., 2015), as well as the potential to co-incorporate synergistic drugs and additional genetic material.

Herein, our objective was to develop a lipid NP (LNP)-based construct capable of efficiently incorporating and delivering mRNA to alveolar epithelial cells and fibroblasts in lungs undergoing fibrosis (Fig. 1). LNP constituent materials were principally selected on the basis of their contribution to NP stability and genetic material incorporation. DOTAP was selected based on its positive charge, making it suitable for concentrating anionic mRNA (Simberg et al., 2004). Similarly, DLin-MC3-DMA was chosen due to its ionizable form that can further increase mRNA concentration in LNPs, and for its role in enhancing endosomal escape (Maugeri et al., 2019). The phospholipid DPPC was chosen to fulfill a structural role given its high stability (Hąc-Wydro and Dynarowicz-Łątka, 2006), as well as its ability to fuse with cell and endosomal membranes (Li and Szoka, 2007). Cholesterol was incorporated to further enhance LNP stability through improved membrane rigidity and integrity (Meng et al., 2021; Hajj and Whitehead, 2017). Moreover, cholesterol incorporation in LNPs is associated with higher transfection efficiencies, likely due to enhanced endosomal escape owing to its crystalline form on LNP surfaces that can promote membrane fusion (Patel et al., 2020). Lastly, the phospholipid-polymer conjugate DSPE-PEG, well known for its biocompatibility and biodegradability (Che et al., 2015), was included in LNPs, with PEGylation of NPs proving advantageous for lung-specific drug and gene delivery applications (Osman et al., 2018; Schuster et al., 2013; Shen et al., 2015). LNPs capable of effectively encapsulating mRNA were fabricated and characterized for size and surface charge, as well as mRNA loading efficiency and release. mRNA-containing LNPs were small (~34 nm), and effectively protected mRNA, which was released in a sustained fashion over time. Following administration to human primary alveolar epithelial cells and lung fibroblasts, mRNA-containing LNPs demonstrated high transfection efficiencies in a time-

and dose-dependent manner. Upon intratracheal delivery in a bleomycin mouse model of lung fibrosis, luciferase mRNA LNPs demonstrated efficacious, site-specific transfection in diseased lungs, as evidenced by robust and prolonged bioluminescent signal *in vivo*. Importantly, fluorescently-tagged mRNA was found co-localized with alveolar epithelial cells, including AEC2, and fibroblasts. Findings from this study demonstrate the potential for nanotherapeutic gene delivery specifically to alveolar epithelial cells and fibroblasts in lungs undergoing fibrosis, opening several avenues for novel treatments in IPF and other ILDs.

2. Materials and Methods

2.1. Materials

1,2-dioleoyl-3-trimethylammonium-propane (DOTAP), 1,2-dipalmitoyl-sn-glycero-3-phosphocholine (DPPC), 1,2-distearoyl-sn-glycero-3-phosphoethanolamine-N-[amino(polyethylene glycol)-2000] (DSPE-PEG), and cholesterol were purchased from Avanti Polar Lipids (Alabaster, AL). (6Z,9Z,28Z,31Z)-heptatriacont-6,9,28,31-tetraene-19-yl 4-(dimethylamino)butanoate (DLin-MC3-DMA) was purchased from Cayman Chemicals (Ann Arbor, MI). Enhanced green fluorescent protein (eGFP) and Cy5-labeled Luciferase (Cy5-Luc) mRNA were obtained from TriLink BioTechnologies (San Diego, CA). Fetal Bovine Serum (FBS) was obtained from Thermo Fisher Scientific (Waltham, MA). Human A549 alveolar epithelial cells, human MRC-5 fibroblast cells, human primary small airway epithelial cells, and human primary lung fibroblasts were purchased from American Type Culture Collection (ATCC, Manassas, VA). Cells were cultured in F12-K and EMEM medium, respectively, and supplemented with 1% (v:v) penicillin/streptomycin (Thermo Fisher Scientific) in a humidified incubator with 5% CO_2 at 37° C. Bleomycin was obtained from Vizient, Inc. (Irving, TX). Unless otherwise specified, all other chemicals and reagents were obtained from Sigma-Aldrich (St. Louis, MO).

2.2. mRNA-containing LNP fabrication and characterization

DOTAP, DLin-MC3-DMA, DPPC, and cholesterol were dissolved in ethanol at a final concentration of 10 mg/mL, DSPE-PEG at a concentration of 5 mg/mL, and final molar ratios established as shown in Table 1. eGFP and Cy5-Luc mRNA were dissolved in nuclease free water prior to LNP fabrication. mRNA-containing LNPs were prepared by combining the lipid and mRNA solutions in a NanoAssemblr™ microfluidic cartridge (Precision NanoSystems, Vancouver, BC) at a speed of 12 mL/min and volumetric ratio of 3:1, followed by removal of ethanol via dialysis (Mw cut-off 3,500 Da). LNPs were then concentrated with Amicon centrifugal filter units (10 kDa cutoff, Sigma-Aldrich).

Physicochemical properties of size, zeta potential, and polydispersity index (PDI) were examined by dynamic light scattering (DLS, Malvern Zetasizer, Worcestershire, UK). mRNA concentration in LNPs and encapsulation efficiency of LNPs were determined by modified fluorescent Quant-iT™ RiboGreen™ RNA Assay (Thermo Fisher Scientific) (Jones et al., 1998). Encapsulation efficiency was determined using the following equation:

$$encapsulation\ \% = \frac{total\ mRNA - free\ mRNA}{total\ mRNA}$$

2.3. Cryo-electron microscopy imaging of LNPs

Cryogenic-transmission electron microscopy (Cryo-TEM) analysis of empty and eGFP mRNA LNPs was performed by the Baylor College of Medicine Cryo-Electron Microscopy Core Facility (Houston, TX). A PELCO easiGlow™ Glow Discharge Cleaning System (Ted Pella, Inc., Redding, CA) was used to glow discharge Quantifoil R1.2/1.3 300 mesh copper grids (Quantifoil Micro Tools GmbH, Jena, DE) for a duration of 20 s at a current of 15 μA. Grids were then transferred to a Vitrobot Mark IV System (Thermo Fisher Scientific, Hillsboro, OR) where 3.5 μL of sample was applied to the grid inside of a chamber maintained at 22° C and 100% humidity to reduce evaporative loss of the aliquot, followed by filter paper blotting. Following blotting, the grids were immediately plunged into liquid ethane cooled by liquid nitrogen and transferred to a grid storage button under liquid nitrogen prior to transfer to a Thermo Fisher Glacios Electron Microscope (Thermo Fischer Scientific) operating at 200 kV. Images were captured using the built-in EPU and Velox programs, and further image analyses was performed using the Fiji/ImageJ software package (NIH).

2.4. Effect of mRNA-containing LNPs on cell viability

Cells (A549, human primary small airway epithelial cells, and human primary lung fibroblasts) were seeded in a 96 multiwell plate (8×10^3/well) and cultured overnight in F12-K medium containing 10% of fetal bovine serum and supplemented with 1% (v:v) penicillin/streptomycin. The following day, medium was replaced with 100 μL of serum free medium containing eGFP mRNA LNPs or lipofectamine 2000 (Thermo Fisher Scientific) at different concentrations and cells were incubated for 24 h. After removing medium, 100 μL of fresh medium containing 0.5 mg/mL of tetrazolium salt 3-(4,5-dimethylthiazol-2-yl)-2,5 diphenyltetrazolium bromide (Invitrogen, Waltham, MA) was added and incubated at 37°C. After 2 h, medium was removed and 100 μL of DMSO were added in each well and incubated for 30 min at RT. The measurements of UV-visible absorptions of all samples were made at 570 nm. Cell viability (%) was calculated using the following formula: $(A_{sample})/(A_{non\text{-}treated}) \times 100$.

2.5. mRNA binding to LNPs and release

RNA binding to lipids was evaluated at different lipids/mRNA molar ratio with EMSA assay using a 1x Tris-acetate-EDTA (TAE) supplemented with 6% agarose gel and RNA was stained with SYBR® Gold Nucleic Acid Gel Stain (Thermo Fisher Scientific). Additionally, mRNA-loaded LNPs were examined for the ability to retain and protect mRNA in the presence of RNase (Thermo Fisher Scientific) at a concentration of 5 U/μl and/or 1% Triton X-100 for 15 min at 37°C. Imaging was performed with a ChemiDocTM XRS+ gel imaging system (BioRad, Hercules, CA). The aforementioned assay was also used to evaluate mRNA binding to LNPs. RNA release from LNPs was performed at pH 5.0 and 7.4 for 7 d based on a previously published procedure (Palama et al., 2015).

2.6. mRNA transfection evaluation

LNP-based eGFP mRNA transfection at different timepoints (6, 24, and 48 h) and concentrations (0.25, 0.5, and 1 μg/mL) was evaluated in human primary small airway epithelial cells, human primary lung fibroblasts, and A549 and MRC-5 cells. mRNA in Lipofectamine RNAi-MAX (ThermoFisher Scientific) was used as a positive transfection control. Transfection efficiency was examined using a BD LSRII Flow Cytometer (BD Biosciences, San Jose, CA) as published previously (Mu et al., 2019).

For confocal microscopy experiments, alveolar epithelial cells (A549 and human primary small airway epithelial cells, 10×10^4 cells/well) and fibroblasts (MRC-5 cells and human primary lung fibroblasts, 8×10^4 cells/well) were seeded in 8-well culture chamber slides in F-12K medium. Following treatment and prior to microscopic examination, cells were fixed, and the nuclei and the cytoskeleton stained with DAPI and Acti-stain™555 (Cytoskeleton, Inc., Denver, CO), respectively. Imaging was performed with a Nikon A1 Confocal Imaging System (Nikon Inc., Melville, NY).

After eGFP mRNA LNP treatment of cells (A549 cells, 12×10^5 cells/well), total protein was extracted from cells to evaluate eGFP expression via Western blot. Briefly, Cells were washed twice with cold PBS and lysate with RIPA buffer (GenDEPOT, Katy, TX) supplemented with 1% of protease/phosphatase inhibitor cocktail (Cell Signaling, Danvers, MA). Proteins were loaded on 4-20% mini-PROTEAN TGX precast gels (BioRad, Hercules, CA), transferred onto an Immun-Blot® PVDF Membrane (BioRad), which was blocked with 5% BSA in TBST 1x. Rabbit GFP antibody (Cell Signaling) was diluted 1:1,000 prior to overnight incubation. Secondary antibody anti-rabbit (Cell Signaling) was added after membrane washing. Imaging was performed with a ChemiDoc™ XRS+ gel imaging system.

2.7. Lysosomal escape studies

Cells (A549, MRC-5) cultured in 10% FBS-containing medium were treated with Cy5-Luc mRNA LNPs (1 μg/mL). After 6 h, LysoTracker Red DND-99 was added for 15 min and cells were fixed with 4% PFA. Nuclei and cytoskeleton were stained with DAPI and Alexa Fluor 488-phalloidin, respectively, followed by confocal microscopy imaging with a Nikon A1 Confocal Imaging System.

2.8. Bleomycin mouse model of lung fibrosis

All animal studies were approved by the Institutional Animal Care and Use Committee of the Houston Methodist Research Institute. Male C57BL/6J mice (7-8 weeks old) were purchased from Jackson Laboratory (Bar Harbor, ME). Mice were treated with bleomycin (0.035 U kg/bw) intraperitoneally (IP) twice a week for a duration of 3 weeks, following a previously published protocol (Headley et al., 2018).

2.9. mRNA-containing LNP delivery to bleomycin-treated mice

At a timepoint of 14 days after model induction, mice (N=5) underwent intratracheal (IT) administration of Cy5-Luc mRNA LNPs at a dose of 1.5 mg/kg mRNA. At timepoints of 2, 24, 48, 72 and 168 h, D-luciferin (15 mg/mL, Gold Biotechnology, St. Louis, MO) was administered IP to mice and whole-body bioluminescence imaging was performed using an

IVIS Spectrum In-Vivo Imaging System (PerkinElmer Inc, Waltham, MA) with exposure times of 0.5 and 60 sec for Cy5-fluorescence and luminescence detection, respectively. Mice were euthanized 7 d after LNP administration.

2.10. In vivo mRNA distribution among alveolar epithelial cells and fibroblasts

In a separate cohort of bleomycin-treated mice, mice (N=3) were sacrificed at a timepoint of 24 h for flow cytometry analysis and immunofluorescence imaging studies. Lungs were inflated with OCT/PBS 1:1 and immediately stored at −80°C. Lung tissue was used to quantitatively determine the cell distribution of LNPs based on a previously published procedure (Singer et al., 2016). Briefly, portions of lung tissue (~170 mg) were minced into a homogenous paste (<1 mm) and transferred to a dissociation medium composed of collagenase/-hyaluronidase and DNase I solution (STEMCELL Technologies Inc., Vancouver, CA) in RPMI medium. Digested lung tissue was then strained and further digested and filtered using 70 μm nylon mesh strainers (Greiner Bio-One, Kremsmünster, AT). Following centrifugation at 300 x g for 10 min at RT, 5 mL of ammonium chloride solution (IBIS Scientific, Las Vegas, NV) was added to the cell pellet and mixed gently. The solution was then incubated on ice for 15 min and centrifuged once more at 300 x g for 10 min. The cell pellet was then resuspended in PBS 1X containing 2% FBS and 0.5% BSA and primary antibodies for 30 min on ice. Lung fibroblasts, alveolar epithelial cells type 1 (AEC1), and AEC2 cells were stained with anti-FSP1 (MilliporeSigma, Burlington, MA) labeled with Zenon Rabbit IgG Alexa Fluor 555 (Thermo Fisher Scientific), FITC-conjugated anti-APQ5 (Novus Biologicals, Littleton, CO), and anti-SFTPC labeled with Zenon Rabbit IgG Alexa Fluor 405 (Thermo Fisher Scientific), respectively. The presence of Cy5-Luc mRNA in alveolar epithelial cells and lung fibroblasts was evaluated by flow cytometry. Lung fibroblasts were first gated for FSP1 expression, and FSP1-negative cells were analyzed for expression of AQP5 (AEC1) and SFTPC (AEC2).

2.11. Immunofluorescence imaging of mRNA in lungs of bleomycin-treated mice

Lung tissue was sliced into 20 μm sections using a CryoStar NX50 (Epredia, Portsmouth, NH). Slides were then fixed in PFA 4% and blocked using 10% goat serum in 0.2% Triton X-100/PBS 1X. Anti-AQP5 (Novus Biotechnology) and anti-SFTPC (EpigenTek, Farmingdale, NY) were used at dilution 1:1000 for AEC1 and AEC2 staining, respectively. Lung fibroblasts were stained with FSP-1 antibody (MilliporeSigma) at a dilution of 1:750. Nuclei were stained with DAPI. Imaging was performed with a Nikon A1 Confocal Imaging System.

3. Results and Discussion

3.1. mRNA-containing LNP fabrication and characterization

LNP systems represent a sophisticated platform for the delivery of a variety of genetic material, including DNA, siRNA, mRNA, and gene-editing complexes (Witzigmann et al., 2020). Our objective herein was to examine LNP delivery of mRNA in *in vitro* and *in vivo* scenarios pertinent to pulmonary fibrosis for eventual modulation of therapeutic protein expression. Varying formulations of LNPs were initially tested to determine efficacious design components that would ensure enhanced mRNA transfection. Table 1 highlights the

distinct lipid and sterol components used among all LNP formulations, the different ratios explored in each, and the physicochemical properties of LNP formulations. DOTAP, one of the most extensively used cationic lipids for applications involving gene transfection (Simberg et al., 2004), and DLin-MC3-DMA, previously shown to be a potent ionizable cationic lipid in gene therapy applications (Jayaraman et al., 2012), were principally used for ionic interaction with mRNA to ensure increased loading efficiencies. Examination of different molar ratios of lipid (DOTAP) to mRNA (N/P ratio) showed complexation at ratios of 5:1, 10:1, 20:1, and 30:1 (Supplementary Fig. S1), with an N/P ratio of 10:1 ultimately selected for further studies. DPPC was incorporated into LNPs to promote fusion with cell and endosomal membranes (Li and Szoka, 2007), while cholesterol proves important for vesicle stability (Eygeris et al., 2020). Lastly, DSPE-PEG, well known for its biocompatibility, biodegradability, and potential for further functionalization (Che et al., 2015) was also incorporated into LNPs. Notably, PEGylation has been previously shown to prolong lung residence times and increase lung coverage of nano- and microparticles after IT administration (Osman et al., 2018; Shen et al., 2015), due largely to evasion of uptake by inflammatory cells (Shen et al., 2015). Osman et al. demonstrated that PEGylated NPs reached a lung coverage of 70% after IT administration, while non-PEGylated NPs were found in less than 40% of the lung parenchyma (Osman et al., 2018). Contrary to non-PEGylated counterparts, PEGylated particles were found in lungs 28 days after IT delivery, with no evidence of inflammatory response (Shen et al., 2015). PEGylation has also been examined as a strategy to overcome mucus penetration, with Schuster et al. demonstrating that PEGylated NPs of 100 and 200 nm in size penetrated respiratory mucus at rates of ~15- and ~35-fold higher than non-PEGylated counterparts, respectively (Schuster et al., 2013). Importantly, PEG amount also affects NP stability. Given the hydrophilic nature of PEG chains, a hydrated cloud with a large exclusion volume is generated on the surface of the NP that prevents interactions with neighboring NPs (Edwards and Almgren, 1992). However, findings by Kirpotin et al. showed a recommended upper PEG molar ratio threshold of 5.7%, above which NP morphology is compromised as the PEG chains lose their brush conformation, resulting in NP aggregation (Kirpotin et al., 1997). As PEGylation increases above 3.5% PEG, so does NP membrane permeability, which adversely affects therapeutic encapsulation efficiency (Nicholas et al., 2000). Importantly, for purposes of cell internalization and transfection, increasing the PEG density may shield the LNP surface charge (Kumar et al., 2014), limiting interaction with negative cell membranes and cell uptake (Verma and Stellacci, 2010). The different formulations were evaluated for size (Table 1, Fig. 2a, Supplementary Fig. S2), surface charge (Table 1, Fig. 2c, Supplementary Fig. S3), PDI (Table 1), encapsulation efficiency (Table 1, Fig. 2d, Supplementary Fig. S4), and cell viability (Table 1, Supplementary Fig. S5). Formulation 5 demonstrated a significantly higher transfection efficiency (92%) compared to other formulations (Supplementary Fig. S6), and a favorable toxicity profile compared to commercial transfection reagents (Supplementary Fig. S5) in A549 cells. Formulation 5 LNPs were also well tolerated in human primary alveolar epithelial cells and lung fibroblasts, with minimal detrimental effect on cell viability at low doses of mRNA-containing LNPs (Supplementary Fig. S7). Considering this, Formulation 5 was used for further studies.

Based on the lipid and cholesterol constituent ratios comprising Formulation 5, LNPs containing mRNA encoding eGFP and Cy5-Luc mRNA were formulated for *in vitro* cell studies and *in vivo* transfection evaluation in a mouse model of lung fibrosis, respectively. eGFP mRNA LNPs measured 34.2 ± 0.8 nm in diameter as determined by DLS, while the size of Cy5-Luc mRNA LNPs were 38.8 ±1.3 nm (Fig. 2a). Cryo-TEM analysis of mRNA-containing LNPs (Fig. 2b) and empty LNPs (Supplementary Fig. S8) showed a size concurrent with DLS results, as well as a spherical morphology and electron dense core that agrees with previously published LNP structure studies (Carrasco et al., 2021; Leung et al., 2012; Mukherjee et al., 2020). Zeta potential analysis showed that the surface charge of eGFP mRNA LNPs was 11.5 ± 2.4 mV, while that of Cy5-Luc mRNA LNPs measured 7.4 ± 1.4 mV (Fig. 2c), both falling within an approximately neutral range, far from either strongly anionic or strongly cationic electrostatic potential (Clogston and Patri, 2011). Lastly, the low PDI of Formulation 5 (0.29 ± 0.08) was indicative of a monodisperse nanoparticle formulation.

Physicochemical properties of NPs such as size, shape, and surface charge have vast implications for cell internalization (Foroozandeh and Aziz, 2018). In a study by Jiang et al, cell uptake was shown to be highest when NPs fell within a size range of 25-50 nm, with spherical NPs exhibiting an ~500% increase in internalization compared to equivalent-sized rod-shaped NPs (Jiang et al., 2008). Lindfors and coworkers recently showed that LNPs measuring ~65 nm underwent more internalization than larger and smaller sized LNPs within 1 h after administration, and that this size yielded the highest intracellular protein production (Arteta et al., 2018). Surface charge of NPs also affects cellular uptake, with negatively-charged NPs undergoing less internalization than positively-charged NPs (Bannunah et al., 2014), owing to the favorable interaction of these NPs with negatively-charged phospholipids in the cell membrane (Voigt et al., 2014). In the context of gene therapy, this property of LNPs addresses a major limitation of mRNA delivery to cells, which is the negative charge of mRNA that precludes its translocation through the negatively-charged membrane (Zeng et al., 2020). Importantly, high transfection efficiencies were recently found to be dependent on early endosomal escape, before sequestration into lysosomes and exocytosis (Sayers et al., 2019). The presence of positively-charged lipid components thus proves advantageous, given that endosomal anionic phospholipid interactions with cationic lipids in nucleic acid–cationic lipid complexes have been shown to disrupt the endosomal membrane and promote cytoplasmic release of genetic material (Hafez et al., 2001). Lastly, both eGFP and Cy5-Luc mRNA LNP formulations incorporated mRNA to a high degree, with loading efficiencies of 85.5 ± 5.3% and 72.9 ± 11.5%, respectively (Fig. 2d), agreeing well with previously published findings regarding mRNA loading efficiencies in LNPs (Kauffman et al., 2016).

Another major limitation of *in vivo* mRNA therapy is instability due to RNase-induced enzymatic degradation (Zeng et al., 2020). Given that intact mRNA must reach the cytosol for translation, adequate protection against ubiquitous RNases throughout the body is vital to the success of mRNA strategies. LNPs are meant to bestow protection to sequestered mRNA within lipid cores. Herein, mRNA housed within LNPs was wholly protected from RNase degradation, in direct contrast to free mRNA (Fig. 3a). mRNA was well housed within LNPs, with mRNA only released and migrating in the presence of the detergent

Triton X-100 that was used to break apart the LNPs. It was only upon the addition of Triton X-100, and in the presence of RNase, that mRNA was degraded. These findings agree with previous reports regarding LNP protection of genetic material. Leung et al. demonstrated that LNPs fully protected encapsulated siRNA from external RNase, and that degradation only occurred in the presence of Triton X-100 (Leung et al., 2012). Mandl and coworkers also showed that LNPs protected a self-amplifying RNA from RNase degradation (Geall et al., 2012). Successful protection of genetic cargo should translate to enhanced mRNA bioavailability at the site of interest and increased translation of therapeutic proteins. mRNA release was conducted at physiological (pH 7.4) and a lower (pH 5.0) pH associated with endosomal compartments (Maxfield, 2014). As can be seen in (Fig. 3)b, release of genetic material from LNPs was negligible during the first 2 h. Release of mRNA was detected at a timepoint of 8 h, with release in pH 5.0 (4.7%) proving faster than release in pH 7.4 (1.3%). A much greater difference in release was observed at a timepoint of 24 h, where release of mRNA in pH 5.0 was ~12.0% compared to ~2.9% in pH 7.4. After 24 h, the rate of release of mRNA from LNPs increased, reaching ~41.4% at 72 h in pH 5.0. Similar mRNA release kinetics over time were observed in LNPs in pH 7.4, although at lesser amounts compared to LNPs in pH 5.0. By 4 d, ~50.8% of mRNA had been released from LNPs in pH 5.0 compared to ~36.2% from LNPs in pH 7.4. Akin to earlier timepoints, mRNA release was faster at pH 5.0 (62.1%) than pH 7.4 (44.2%) at day 5. By day 7, release kinetics seemingly reached a plateau at both pH 5.0 (66.3%) and 7.4 (55.3%). The slow release of mRNA from LNPs at pH 7.4 during the first 24 h (2.9%) proves advantageous for delivery of genetic cargo, offering protection against RNase degradation for a prolonged time after administration and prior to arrival to the site of action. Of note, cumulative mRNA release from LNPs throughout the course of the study proved more elevated at pH 5.0, suggesting a more rapid release of mRNA may occur in endosomal compartments whose pH is reduced from 6.8 to 4.5 as they transition to lysosomes (Huotari and Helenius, 2011). Promoting endosomal escape represents an important LNP design consideration, with findings suggesting that lower ionizable lipid and cholesterol amounts and elevated helper lipid amounts result in optimal mRNA delivery to the cytoplasm for translation (Kauffman et al., 2015).

3.2. mRNA transfection of alveolar epithelial cells and fibroblasts in vitro

The transfection efficiency of LNPs housing mRNA expressing eGFP was examined in human primary alveolar epithelial cells and lung fibroblasts, as well as A549 human alveolar basal epithelial cells and MRC-5 human fibroblasts, quantitatively using flow cytometry analysis and qualitatively via confocal microscopy. eGFP expression was evident in A549 cells at an early timepoint of 6 h at a low dose of 0.25 μg/mL, with ~16% transfection (Supplementary Fig. S9). And while eGFP expression was present in cells at 6 h, and transfection proved to be dose-dependent, only 61.9% transfection was observed at a dose of 1 μg/mL. Limited eGFP expression at this early timepoint may be the result of time constraints related to LNP cell internalization (Ruiz de Garibay et al., 2013) and endosomal uptake and release, with previous mRNA expression kinetics studies showing an expression onset at ~3 h after transfection (Leonhardt et al., 2014). Notably, mRNA-containing LNPs and lysosomes showed minimal co-localization at this timepoint (Supplementary Fig. S10). At later timepoints, eGFP transfection proved dose- and time-dependent following LNP

administration (Fig. 4a). At a concentration of 0.25 μg/mL of eGFP mRNA, time after administration proved the major determinant of increased transfection in human primary alveolar epithelial cells (38.3% at 24 h compared to 58.4% at 48 h). At a higher dose of 1 μg/mL of eGFP mRNA, time was no longer a factor influencing transfection, as cells treated with mRNA-containing LNPs for timepoints of 24 and 48 h had near equivalent transfection efficiencies of 95.1% and 96.0%, respectively. A similar trend was observed in human primary lung fibroblasts, in which the lowest concentration (0.25 μg/mL) efficiently transfected only 34.9% of cells after 24 h. However, the same RNA concentration led to eGFP expression in 49.9% of cells at 48 h. At a higher concentration of 0.5 μg/mL of eGFP mRNA, transfection still proved time-dependent, as 69.8% and 82.6% of cells were transfected at 24 and 48 h, respectively. Lastly, transfection was no longer time-dependent at the highest dose (1 μg/mL), as equivalent number of cells (~93%) expressed eGFP at 24 and 48 h. Successful transfection of eGFP mRNA in human primary alveolar epithelial cells and lung fibroblasts at 24 and 48 h after LNP treatment was corroborated via confocal microscopy, showing clear eGFP expression in the majority of cells (Fig. 4b). LNP transfection efficiency findings in human primary alveolar epithelial cells and lung fibroblasts were very similar in A549 and MRC-5 cells (Supplementary Fig. S11). Dose- and time-dependent effects of mRNA transfection were also observed via Western blot analysis, with 24 and 48 h timepoints demonstrating heightened eGFP protein expression compared to the 6 h timepoint (Supplementary Fig. S12). The favorable kinetics and extent of mRNA transfection via the LNP platform in these cells was expected to translate to efficacious protein translation in the *in vivo* setting.

3.3. In vivo delivery of mRNA-containing LNPs in a bleomycin mouse model of lung fibrosis

Our ultimate objective was to evaluate the delivery of mRNA in lungs undergoing fibrosis, with the goal of highlighting the potential for gene therapy as a viable treatment option. Current pharmacotherapies have limited efficacy in IPF patients. Two antifibrotic drugs, pirfenidone and nintedanib, have been shown clinically to slow the deterioration in lung function and IPF progression, but potential harmful side-effects exist and there is no clear evidence concerning improvements in long-term mortality (Canestaro et al., 2016). Mechanistic insights into the pathogenesis and progression of IPF have resulted in several avenues for molecular target modulation, specifically the ability to restore or enhance the expression of specific proteins via synthetic mRNAs (Sahin et al., 2014). LNPs have recently enabled effective translation of RNA therapeutics from the *in vitro* setting into the clinical arena. Patisiran (Onpattro) is an RNAi-based therapy approved for hereditary transthyretin amyloidosis after patients showed improvements in multiple clinical manifestations of the disease (Adams et al., 2018). Most recently, the mRNA-1273 vaccine, an mRNA-based LNP construct, showed ~94% efficacy at preventing Covid-19 illness and severe disease (Baden et al., 2021), highlighting the immense potential for NP-mediated mRNA treatments in a variety of diseases. Successful transfection in alveolar epithelial cells and fibroblasts *in vitro* (Fig. 4) led us to evaluate the efficacy of mRNA-containing LNPs in a mouse model of lung fibrosis. Cy5-Luc mRNA LNPs were formulated and following IT delivery in a bleomycin mouse model of lung fibrosis, mouse lungs were examined for epifluorescence and luminescence. mRNA-associated fluorescence was evident in mouse

lungs 2 h after IT administration (Fig. 5a). Of note, examination of epifluorescence from distinct organs (liver, spleen, kidneys, and heart) at a timepoint of 24 h after administration showed no presence of mRNA in organs other than lungs (Supplementary Fig. S13), highlighting the potential of the IT route for site-specific delivery. Fluorescence associated with mRNA was present in the lungs at the earliest timepoint of 2 h and in a sustained fashion throughout the course of 48 h after IT administration of LNPs (Fig. 5a).

Importantly, Cy5-Luc mRNA was translated to functional protein at the 2 h timepoint, resulting in a bioluminescent signal that proved very strong at the 24 h timepoint (Fig. 5a). Analysis of the kinetics of bioluminescence showed that luminescence emanating from lungs of mice undergoing fibrosis increased at 2 h to a value of 29191.6 ± 16306.9 counts prior to peaking at a timepoint of 24 h (203185.3 ± 21234.9 counts) (Fig: 5b). The signal abated at 48 h to a value of 49157.5 ± 16571.0 counts and there was no measurable luciferase activity at a timepoint of 72 h (Supplementary Fig. S14). Results regarding translational kinetics varied slightly with previously published findings involving IT delivery of luciferase mRNA-containing LNPs in healthy mice. Pardi et al. demonstrated that bioluminescent signal in healthy BALB/c mice following IT administration of luciferase mRNA LNPs peaked at 4.8 h with minimal activity detected at 2 and 3 d at low and high doses, respectively (Pardi et al., 2015). In a recent study by Ghosh and coworkers, IT delivery of LNPs containing luciferase mRNA in BALB/c mice resulted in a peak in bioluminescence signal from lungs at a timepoint of 6 h after administration (Zhang et al., 2020).

As mentioned previously, alveolar epithelial cells and fibroblasts represent important drivers of fibrosis in IPF. Injury to alveolar epithelial cells and their dysfunction consists of an early initiating event that contributes to fibroproliferation in IPF and eventual loss of lung function (Parimon et al., 2020). Moreover, AEC2 release factors and mediators that can contribute to fibroblast migration, proliferation, and differentiation into myofibroblasts, with activated myofibroblasts proving crucial for excessive deposition of ECM in IPF (Moore and Herzog, 2013). Thus, mRNA therapeutics targeting alveolar epithelial cells and fibroblasts represent viable treatment modalities in IPF. Examination of lungs from bleomycin-treated mice demonstrated that at a timepoint of 24 h after IT administration, Cy5-Luc mRNA was found associated with alveolar epithelial cells and fibroblasts (Fig. 6). Flow cytometry analysis of lungs showed that LNPs were able to deliver mRNA to alveolar epithelial cells, notably AEC2, and fibroblasts (Fig. 6a), and these findings agreed with confocal microscopy examination of lungs (Fig. 6b).

Results highlight the feasibility of directing mRNA therapeutics to alveolar epithelial cells and fibroblasts in lung fibrosis. To the best of our knowledge, *in vivo* mRNA delivery specifically to lungs undergoing fibrosis using LNP technologies has not been explored previously. Recently, Zhang et al. used a nanoformulation comprised of a ribosomal protein-condensed mRNA core to enhance expression of matrix metallopeptidase 13 (MMP13), ameliorating disease progression in a bleomycin mouse model of lung fibrosis (Zhang et al., 2022). Expression enhancement of specific genes in alveolar epithelial cells and fibroblasts in mouse models of lung fibrosis has been explored previously primarily using viral vectors to deliver plasmid DNA (pDNA) (Ruigrok et al., 2021). Inoshima et al.

showed that adenoviral delivery of the p21 gene resulted in a fewer number of apoptotic alveolar epithelial cells, and decreased lung inflammation and fibrosis in a bleomycin mouse model of lung fibrosis (Inoshima et al., 2004). Kim and coworkers showed that adenoviral-mediated overexpression of inhibitor of DNA-binding 2 (Id2), a transcription factor that blocks TGF-β-induced collagen type I expression, resulted in alveolar epithelial cell proliferation and reduced fibrosis in bleomycin-treated mice (Yang et al., 2015). Huang et al. observed that expression of fetal-lethal noncoding developmental regulatory RNA (FENDRR) was downregulated in primary lung fibroblasts isolated from a bleomycin mouse model of lung fibrosis, and adenovirus-mediated FENDRR gene transfer improved lung function in these mice (Huang et al., 2020). Our findings, along with previously published reports regarding gene therapy to increase levels of proteins with therapeutic implications, highlight the feasibility of mRNA-based treatments in pulmonary fibrosis.

Herein, we show the potential for NP-based delivery of mRNA therapeutics to lungs undergoing fibrosis. The small-sized LNPs provide for efficient mRNA encapsulation, with efficacious protection against degradation and sustained release of mRNA over time. Importantly, mRNA transfection efficiency *in vitro* proved robust, especially at higher doses and longer times after administration. In a bleomycin mouse model of lung fibrosis, IT administration of mRNA-containing LNPs resulted in site-specific accumulation of the construct in lungs and successful mRNA transfection in alveolar epithelial cells and fibroblasts; attractive target cells for IPF therapy due to their role in disease pathogenesis. In the future, we will explore the delivery of mRNA capable of synthesizing proteins with therapeutic implications in pulmonary fibrosis, with emphasis on efficacy examination in a bleomycin mouse model of lung fibrosis. Moreover, we will evaluate the possibility to deliver mRNA to other cell types involved in IPF progression (e.g. alveolar macrophages). Findings from this study, in particular the ability to transfect mRNA in pulmonary tissue, opens several treatment avenues in other chronic lung diseases.

Supplementary Material

Refer to Web version on PubMed Central for supplementary material.

Acknowledgements

This work was supported by funding from the Houston Methodist Research Institute. The authors thank Rachael Whitehead and Matthew G. Landry for assistance with schematics. The authors acknowledge the Baylor College of Medicine Cryo-Electron Microscopy Core Facility for performing cryo-electron microscopy imaging of LNPs. The authors also acknowledge Dr. David Haviland, director of the Houston Methodist Research Institute Flow Cytometry Core, for assistance with flow cytometry. M.M. is grateful for the economic support kindly provided to him by B.S.P Pharmaceuticals (Latina, IT). G.B. and M.M. received funding support from the ANSO Scholarship for Young Talents, University of Chinese Academy of Sciences, College of Material Science and Opto-electronic Technology.

Data availability

Data will be made available on request.

References

Adams D, Gonzalez-Duarte A, O'Riordan WD, Yang CC, Ueda M, Kristen AV, Tournev I, Schmidt HH, Coelho T, Berk JL, Lin KP, Vita G, Attarian S, Plante-Bordeneuve V, Mezei MM, Campistol JM, Buades J, Brannagan TH 3rd, Kim BJ, Oh J, Parman Y, Sekijima Y, Hawkins PN, Solomon SD, Polydefkis M, Dyck PJ, Gandhi PJ, Goyal S, Chen J, Strahs AL, Nochur SV, Sweetser MT, Garg PP, Vaishnaw AK, Gollob JA, Suhr OB, 2018. Patisiran, an RNAi Therapeutic, for Hereditary Transthyretin Amyloidosis. N. Engl. J. Med 379, 11–21. [PubMed: 29972753]

Arteta MY, Kjellman T, Bartesaghi S, Wallin S, Wu XQ, Kvist AJ, Dabkowska A, Szekely N, Radulescu A, Bergenholtz J, Lindfors L, 2018. Successful reprogramming of cellular protein production through mRNA delivered by functionalized lipid nanoparticles. Proc. Natl. Acad. Sci. U. S. A 115, E3351–E3360. [PubMed: 29588418]

Baden LR, El Sahly HM, Essink B, Kotloff K, Frey S, Novak R, Diemert D, Spector SA, Rouphael N, Creech CB, McGettigan J, Khetan S, Segall N, Solis J, Brosz A, Fierro C, Schwartz H, Neuzil K, Corey L, Gilbert P, Janes H, Follmann D, Marovich M, Mascola J, Polakowski L, Ledgerwood J, Graham BS, Bennett H, Pajon R, Knightly C, Leav B, Deng W, Zhou H, Han S, Ivarsson M, Miller J, Zaks T, Group CS, 2021. Efficacy and Safety of the mRNA-1273 SARS-CoV-2 Vaccine. N. Engl. J. Med 384, 403–416. [PubMed: 33378609]

Bannunah AM, Vllasaliu D, Lord J, Stolnik S, 2014. Mechanisms of nanoparticle internalization and transport across an intestinal epithelial cell model: effect of size and surface charge. Mol. Pharm 11, 4363–4373. [PubMed: 25327847]

Blanco E, Shen H, Ferrari M, 2015. Principles of nanoparticle design for overcoming biological barriers to drug delivery. Nat. Biotechnol 33, 941–951. [PubMed: 26348965]

Canestaro WJ, Forrester SH, Raghu G, Ho L, Devine BE, 2016. Drug Treatment of Idiopathic Pulmonary Fibrosis: Systematic Review and Network Meta-Analysis. Chest 149, 756–766. [PubMed: 26836914]

Carrasco MJ, Alishetty S, Alameh M-G, Said H, Wright L, Paige M, Soliman O, Weissman D, Cleveland TE, Grishaev A, 2021. Ionization and structural properties of mRNA lipid nanoparticles influence expression in intramuscular and intravascular administration. Commun. Biol 4, 1–15. [PubMed: 33398033]

Che J, Okeke CI, Hu ZB, Xu J, 2015. DSPE-PEG: a distinctive component in drug delivery system. Curr. Pharm. Des 21, 1598–1605. [PubMed: 25594410]

Chen NY, Luo DCSF, Weng T, Le TT, Philip MHAK, Molina JG, Garcia-Morales LJ, Cao Y, Ko TC, Amione-Guerra J, Al-Jabbari O, Bunge RR, Youker K, Bruckner BA, Hamid R, Davies J, Sinha N, Karmouty-Quintana H, 2016. Macrophage bone morphogenic protein receptor 2 depletion in idiopathic pulmonary fibrosis and Group III pulmonary hypertension. Am. J. Physiol. Lung Cell. Mol. Physiol 311, L238–L254. [PubMed: 27317687]

Clogston JD, Patri AK, 2011. Zeta potential measurement. Methods Mol. Biol 697, 63–70. [PubMed: 21116954]

Conley SM, Naash MI, 2010. Nanoparticles for retinal gene therapy. Prog. Retin. Eye Res 29, 376–397. [PubMed: 20452457]

Creech CB, Walker SC, Samuels RJ, 2021. SARS-CoV-2 Vaccines. JAMA 325, 1318–1320. [PubMed: 33635317]

Davis ME, Zuckerman JE, Choi CH, Seligson D, Tolcher A, Alabi CA, Yen Y, Heidel JD, Ribas A, 2010. Evidence of RNAi in humans from systemically administered siRNA via targeted nanoparticles. Nature 464, 1067–1070. [PubMed: 20305636]

Douglas JT, 2007. Adenoviral vectors for gene therapy. Mol. Biotechnol 36, 71–80. [PubMed: 17827541]

Edwards K, Almgren M, 1992. Surfactant-induced leakage and structural change of lecithin vesides: effect of surfactant headgroup size. Langmuir 8, 824–832.

Eygeris Y, Patel S, Jozic A, Sahay G, 2020. Deconvoluting Lipid Nanoparticle Structure for Messenger RNA Delivery. Nano Lett. 20, 4543–4549. [PubMed: 32375002]

Foroozandeh P, Aziz AA, 2018. Insight into Cellular Uptake and Intracellular Trafficking of Nanoparticles. Nanoscale Res. Lett 13. [PubMed: 29327154]

Geall AJ, Verma A, Otten GR, Shaw CA, Hekele A, Banerjee K, Cu Y, Beard CW, Brito LA, Krucker T, O'Hagan DT, Singh M, Mason PW, Valiante NM, Dormitzer PR, Barnett SW, Rappuoli R, Ulmer JB, Mandl CW, 2012. Nonviral delivery of self-amplifying RNA vaccines. Proc. Natl. Acad. Sci. U. S. A 109, 14604–14609. [PubMed: 22908294]

Hąc-Wydro K, Dynarowicz-Łątka P, 2006. Interaction between nystatin and natural membrane lipids in Langmuir monolayers—the role of a phospholipid in the mechanism of polyenes mode of action. Biophys. Chem 123, 154–161. [PubMed: 16766114]

Hafez IM, Maurer N, Cullis PR, 2001. On the mechanism whereby cationic lipids promote intracellular delivery of polynucleic acids. Gene Ther. 8, 1188–1196. [PubMed: 11509950]

Hajj KA, Whitehead KA, 2017. Tools for translation: non-viral materials for therapeutic mRNA delivery. Nat. Rev. Mater 2.

Headley L, Bi W, Wilson C, Collum SD, Chavez M, Darwiche T, Mertens TCJ, Hernandez AM, Siddiqui SR, Rosenbaum S, Johnston RA, Karmouty-Quintana H, 2018. Low-dose administration of bleomycin leads to early alterations in lung mechanics. Exp. Physiol 103, 1692–1703. [PubMed: 30260066]

Huang C, Liang Y, Zeng X, Yang X, Xu D, Gou X, Sathiaseelan R, Senavirathna LK, Wang P, Liu L, 2020. Long Noncoding RNA FENDRR Exhibits Antifibrotic Activity in Pulmonary Fibrosis. Am. J. Respir. Cell Mol. Biol 62, 440–453. [PubMed: 31697569]

Huotari J, Helenius A, 2011. Endosome maturation. EMBO J. 30, 3481–3500. [PubMed: 21878991]

Hutchinson J, Fogarty A, Hubbard R, McKeever T, 2015. Global incidence and mortality of idiopathic pulmonary fibrosis: a systematic review. Eur. Respir. J 46, 795–806. [PubMed: 25976683]

Inoshima I, Kuwano K, Hamada N, Yoshimi M, Maeyama T, Hagimoto N, Nakanishi Y, Hara N, 2004. Induction of CDK inhibitor p21 gene as a new therapeutic strategy against pulmonary fibrosis. Am. J. Physiol. Lung Cell. Mol. Physiol 286, L727–L733. [PubMed: 15003936]

Jayaraman M, Ansell SM, Mui BL, Tam YK, Chen J, Du X, Butler D, Eltepu L, Matsuda S, Narayanannair JK, Rajeev KG, Hafez IM, Akinc A, Maier MA, Tracy MA, Cullis PR, Madden TD, Manoharan M, Hope MJ, 2012. Maximizing the potency of siRNA lipid nanoparticles for hepatic gene silencing in vivo. Angew. Chem. Int. Ed Engl 51, 8529–8533. [PubMed: 22782619]

Jiang W, Kim BYS, Rutka JT, Chan WCW, 2008. Nanoparticle-mediated cellular response is size-dependent. Nat. Nanotechnol 3, 145–150. [PubMed: 18654486]

Jones LJ, Yue ST, Cheung CY, Singer VL, 1998. RNA quantitation by fluorescence-based solution assay: RiboGreen reagent characterization. Anal. Biochem 265, 368–374. [PubMed: 9882416]

Kauffman KJ, Dorkin JR, Yang JH, Heartlein MW, DeRosa F, Mir FF, Fenton OS, Anderson DG, 2015. Optimization of Lipid Nanoparticle Formulations for mRNA Delivery in Vivo with Fractional Factorial and Definitive Screening Designs. Nano Lett. 15, 7300–7306. [PubMed: 26469188]

Kauffman KJ, Mir FF, Jhunjhunwala S, Kaczmarek JC, Hurtado JE, Yang JH, Webber MJ, Kowalski PS, Heartlein MW, DeRosa F, Anderson DG, 2016. Efficacy and immunogenicity of unmodified and pseudouridine-modified mRNA delivered systemically with lipid nanoparticles in vivo. Biomaterials 109, 78–87. [PubMed: 27680591]

King TE Jr., Pardo A, Selman M, 2011. Idiopathic pulmonary fibrosis. Lancet 378, 1949–1961. [PubMed: 21719092]

Kirpotin D, Park JW, Hong K, Zalipsky S, Li W-L, Carter P, Benz CC, Papahadjopoulos D, 1997. Sterically stabilized anti-HER2 immunoliposomes: design and targeting to human breast cancer cells in vitro. Biochemistry 36, 66–75. [PubMed: 8993319]

Kumar V, Qin J, Jiang Y, Duncan RG, Brigham B, Fishman S, Nair JK, Akinc A, Barros SA, Kasperkovitz PV, 2014. Shielding of lipid nanoparticles for siRNA delivery: impact on physicochemical properties, cytokine induction, and efficacy. Mol. Ther. Nucleic Acids 3, e210. [PubMed: 25405467]

Lederer DJ, Martinez FJ, 2018. Idiopathic Pulmonary Fibrosis. N. Engl. J. Med 378, 1811–1823. [PubMed: 29742380]

Leonhardt C, Schwake G, Stogbauer TR, Rappl S, Kuhr JT, Ligon TS, Radler JO, 2014. Single-cell mRNA transfection studies: delivery, kinetics and statistics by numbers. Nanomedicine 10, 679–688. [PubMed: 24333584]

Leung AK, Hafez IM, Baoukina S, Belliveau NM, Zhigaltsev IV, Afshinmanesh E, Tieleman DP, Hansen CL, Hope MJ, Cullis PR, 2012. Lipid Nanoparticles Containing siRNA Synthesized by Microfluidic Mixing Exhibit an Electron-Dense Nanostructured Core. J. Phys. Chem. C Nanomater. Interf 116, 18440–18450.

Li W, Szoka FC Jr., 2007. Lipid-based nanoparticles for nucleic acid delivery. Pharm. Res 24, 438–449. [PubMed: 17252188]

Martinez FJ, Collard HR, Pardo A, Raghu G, Richeldi L, Selman M, Swigris JJ, Taniguchi H, Wells AU, 2017. Idiopathic pulmonary fibrosis. Nat. Rev. Dis. Primers 3, 17074. [PubMed: 29052582]

Maugeri M, Nawaz M, Papadimitriou A, Angerfors A, Camponeschi A, Na M, Hölttä M, Skantze P, Johansson S, Sundqvist M, 2019. Linkage between endosomal escape of LNP-mRNA and loading into EVs for transport to other cells. Nat. Commun 10, 1–15. [PubMed: 30602773]

Maxfield FR, 2014. Role of endosomes and lysosomes in human disease. Cold Spring Harb. Perspect. Biol 6 a016931. [PubMed: 24789821]

Meng C, Chen Z, Li G, Welte T, Shen H, 2021. Nanoplatforms for mRNA therapeutics. Adv. Ther 4, 2000099.

Moore MW, Herzog EL, 2013. Regulation and Relevance of Myofibroblast Responses in Idiopathic Pulmonary Fibrosis. Curr. Pathobiol. Rep 1, 199–208. [PubMed: 25705577]

Mu W, Homann S, Hofmann C, Gorin A, Huynh D, Yang OO, Kelesidis T, 2019. A Flow Cytometric Method to Determine Transfection Efficiency. Bio Protoc. 9.

Mukherjee A, MacDonald KD, Kim J, Henderson MI, Eygeris Y, Sahay G, 2020. Engineered mutant alpha-ENaC subunit mRNA delivered by lipid nanoparticles reduces amiloride currents in cystic fibrosis-based cell and mice models. Sci. Adv 6.

Nicholas AR, Scott MJ, Kennedy NI, Jones MN, 2000. Effect of grafted polyethylene glycol (PEG) on the size, encapsulation efficiency and permeability of vesicles. Biochim. Biophys. Acta. Biomembr 1463, 167–178.

Noble PW, Albera C, Bradford WZ, Costabel U, du Bois RM, Fagan EA, Fishman RS, Glaspole I, Glassberg MK, Lancaster L, Lederer DJ, Leff JA, Nathan SD, Pereira CA, Swigris JJ, Valeyre D, King TE Jr., 2016. Pirfenidone for idiopathic pulmonary fibrosis: analysis of pooled data from three multinational phase 3 trials. Eur. Respir. J 47, 243–253. [PubMed: 26647432]

Osman G, Rodriguez J, Chan SY, Chisholm J, Duncan G, Kim N, Tatler AL, Shakesheff KM, Hanes J, Suk JS, Dixon JE, 2018. PEGylated enhanced cell penetrating peptide Nanoparticles for lung gene therapy. J. Control. Release 285, 35–45. [PubMed: 30004000]

Palama IE, Cortese B, D'Amone S, Gigli G, 2015. mRNA delivery using non-viral PCL nanoparticles. Biomater. Sci 3, 144–151. [PubMed: 26214197]

Pardi N, Tuyishime S, Muramatsu H, Kariko K, Mui BL, Tam YK, Madden TD, Hope MJ, Weissman D, 2015. Expression kinetics of nucleoside-modified mRNA delivered in lipid nanoparticles to mice by various routes. J. Control. Release 217, 345–351. [PubMed: 26264835]

Parimon T, Yao CF, Stripp BR, Noble PW, Chen P, 2020. Alveolar Epithelial Type II Cells as Drivers of Lung Fibrosis in Idiopathic Pulmonary Fibrosis. Int. J. Mol. Sci 21. [PubMed: 33375030]

Patel S, Ashwanikumar N, Robinson E, Xia Y, Mihai C, Griffith JP, Hou S, Esposito AA, Ketova T, Welsher K, 2020. Naturally-occurring cholesterol analogues in lipid nanoparticles induce polymorphic shape and enhance intracellular delivery of mRNA. Nat. Commun 11, 1–13. [PubMed: 31911652]

Pedroza M, Le TT, Lewis K, Karmouty-Quintana H, To S, George AT, Blackburn MR, Tweardy DJ, Agarwal SK, 2016. STAT-3 contributes to pulmonary fibrosis through epithelial injury and fibroblast-myofibroblast differentiation. Faseb J. 30, 129–140. [PubMed: 26324850]

Raghu G, Collard HR, Egan JJ, Martinez FJ, Behr J, Brown KK, Colby TV, Cordier JF, Flaherty KR, Lasky JA, Lynch DA, Ryu JH, Swigris JJ, Wells AU, Ancochea J, Bouros D, Carvalho C, Costabel U, Ebina M, Hansell DM, Johkoh T, Kim DS, King TE Jr., Kondoh Y, Myers J, Muller NL, Nicholson AG, Richeldi L, Selman M, Dudden RF, Griss BS, Protzko SL, Schunemann HJ, 2011. An official ATS/ERS/JRS/ALAT statement: idiopathic pulmonary fibrosis: evidence-based guidelines for diagnosis and management. Am. J. Respir. Crit. Care Med 183, 788–824. [PubMed: 21471066]

Richeldi L, Costabel U, Selman M, Kim DS, Hansell DM, Nicholson AG, Brown KK, Flaherty KR, Noble PW, Raghu G, Bran M, Gupta A, Juhel N, Kluglich M, du Bois RM, 2011. Efficacy of a tyrosine kinase inhibitor in idiopathic pulmonary fibrosis. N. Engl. J. Med 365, 1079–1087. [PubMed: 21992121]

Ruigrok MJR, Frijlink HW, Melgert BN, Olinga P, Hinrichs WLJ, 2021. Gene therapy strategies for idiopathic pulmonary fibrosis: recent advances, current challenges, and future directions. Mol. Ther. Methods Clin. Dev 20, 483–496. [PubMed: 33614824]

Ruiz de Garibay AP, Solinis Aspiazu MA, Rodriguez Gascon A, Ganjian H, Fuchs R, 2013. Role of endocytic uptake in transfection efficiency of solid lipid nanoparticles-based nonviral vectors. J. Gene Med 15, 427–440. [PubMed: 24339018]

Sahin U, Kariko K, Tureci O, 2014. mRNA-based therapeutics–developing a new class of drugs. Nat. Rev. Drug Discov 13, 759–780. [PubMed: 25233993]

Sayers EJ, Peel SE, Schantz A, England RM, Beano M, Bates SM, Desai AS, Puri S, Ashford MB, Jones AT, 2019. Endocytic Profiling of Cancer Cell Models Reveals Critical Factors Influencing LNP-Mediated mRNA Delivery and Protein Expression. Mol. Ther 27, 1950–1962. [PubMed: 31427168]

Schuster BS, Suk JS, Woodworth GF, Hanes J, 2013. Nanoparticle diffusion in respiratory mucus from humans without lung disease. Biomaterials 34, 3439–3446. [PubMed: 23384790]

Selman M, Pardo A, 2014. Revealing the pathogenic and aging-related mechanisms of the enigmatic idiopathic pulmonary fibrosis. an integral model. Am. J. Respir. Crit. Care Med 189, 1161–1172. [PubMed: 24641682]

Selman M, Pardo A, 2020. The leading role of epithelial cells in the pathogenesis of idiopathic pulmonary fibrosis. Cell Signal 66, 109482. [PubMed: 31760172]

Shen TW, Fromen CA, Kai MP, Luft JC, Rahhal TB, Robbins GR, DeSimone JM, 2015. Distribution and cellular uptake of PEGylated polymeric particles in the lung towards cell-specific targeted delivery. Pharm. Res 32, 3248–3260. [PubMed: 26002743]

Sheng G, Chen P, Wei Y, Yue H, Chu J, Zhao J, Wang Y, Zhang W, Zhang HL, 2020. Viral Infection Increases the Risk of Idiopathic Pulmonary Fibrosis: A Meta-Analysis. Chest 157, 1175–1187. [PubMed: 31730835]

Simberg D, Weisman S, Talmon Y, Barenholz Y, 2004. DOTAP (and other cationic lipids): chemistry, biophysics, and transfection. Crit. Rev. Ther. Drug Carrier Syst 21, 257–317. [PubMed: 15638468]

Singer BD, Mock JR, D'Alessio FR, Aggarwal NR, Mandke P, Johnston L, Damarla M, 2016. Flow-cytometric method for simultaneous analysis of mouse lung epithelial, endothelial, and hematopoietic lineage cells. Am. J. Physiol. Lung Cell. Mol. Physiol 310, L796–L801. [PubMed: 26944088]

Tokatlian T, Segura T, 2010. siRNA applications in nanomedicine. Wiley Interdiscip. Rev. Nanomed. Nanobiotechnol 2, 305–315. [PubMed: 20135697]

Verma A, Stellacci F, 2010. Effect of surface properties on nanoparticle-cell interactions. Small 6, 12–21. [PubMed: 19844908]

Voigt J, Christensen J, Shastri VP, 2014. Differential uptake of nanoparticles by endothelial cells through polyelectrolytes with affinity for caveolae. Proc. Natl. Acad. Sci. U. S. A 111, 2942–2947. [PubMed: 24516167]

Wang Z, Zhang X, 2021. Adenovirus vector-attributed hepatotoxicity blocks clinical application in gene therapy. Cytotherapy 23, 1045–1052. [PubMed: 34548241]

Witzigmann D, Kulkarni JA, Leung J, Chen S, Cullis PR, van der Meel R, 2020. Lipid nanoparticle technology for therapeutic gene regulation in the liver. Adv. Drug. Deliv. Rev 159, 344–363. [PubMed: 32622021]

Yang JB, Velikoff M, Agarwal M, Disayabutr S, Wolters PJ, Kim KK, 2015. Overexpression of Inhibitor of DNA-Binding 2 Attenuates Pulmonary Fibrosis through Regulation of c-Abl and Twist. Am. J. Pathol 185, 1001–1011. [PubMed: 25661109]

Zeng C, Zhang C, Walker PG, Dong Y, 2020. Formulation and Delivery Technologies for mRNA Vaccines. Curr. Top. Microbiol. Immunol

Zhang HR, Leal J, Soto MR, Smyth HDC, Ghosh D, 2020. Aerosolizable Lipid Nanoparticles for Pulmonary Delivery of mRNA through Design of Experiments. Pharmaceutics 12. [PubMed: 33374646]

Zhang R, Jing W, Chen C, Zhang S, Abdalla M, Sun P, Wang G, You W, Yang Z, Zhang J, Tang C, Du W, Liu Y, Li X, Liu J, You X, Hu H, Cai L, Xu F, Dong B, Liu M, Qiang B, Sun Y, Yu G, Wu J, Zhao K, Jiang X, 2022. Inhaled mRNA Nanoformulation with Biogenic Ribosomal Protein Reverses Established Pulmonary Fibrosis in a Bleomycin-Induced Murine Model. Adv. Mater 34, e2107506. [PubMed: 35146813]

Zhao Y, Huang L, 2014. Lipid nanoparticles for gene delivery. Adv. Genet 88, 13–36. [PubMed: 25409602]

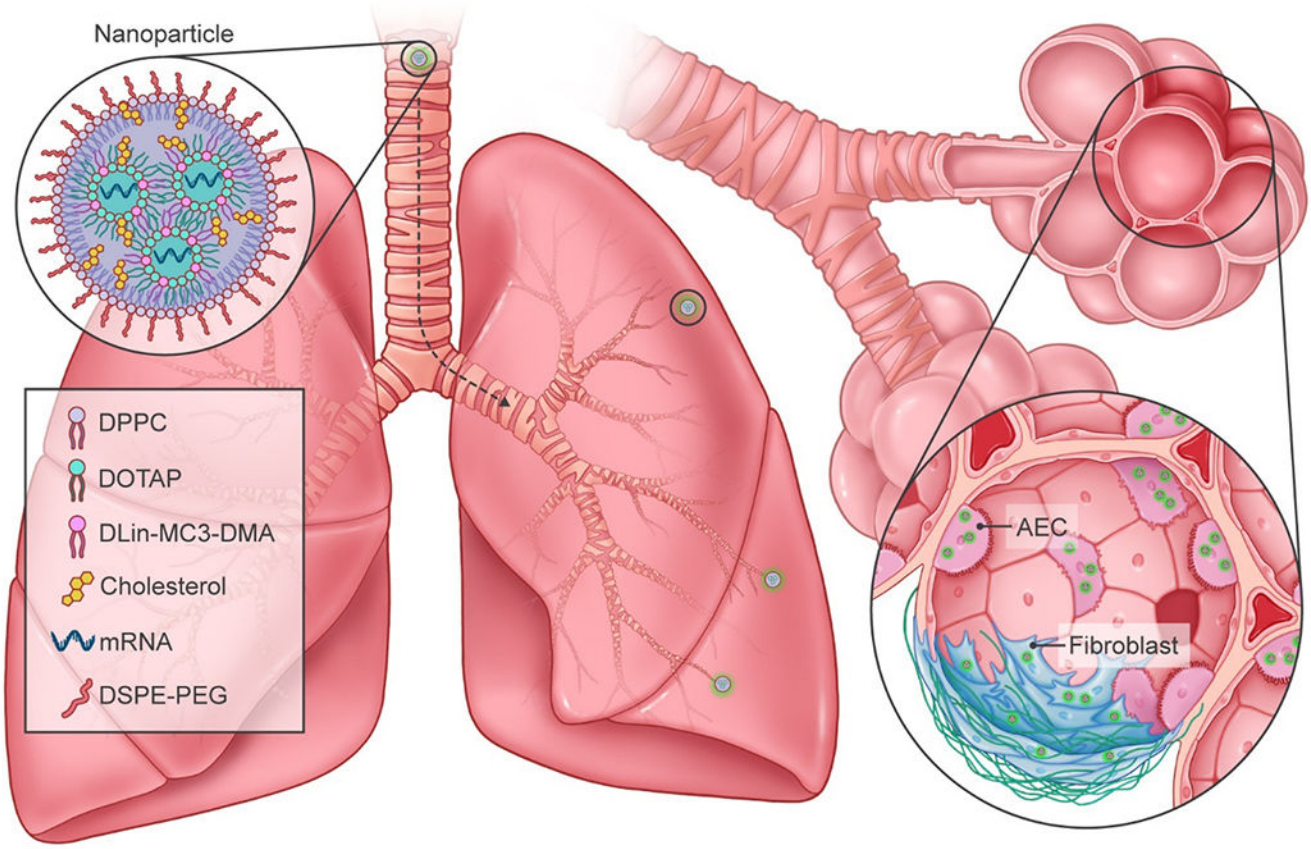

Fig. 1.

Schematic of LNPs for delivery of mRNA to lungs undergoing fibrosis. LNPs comprised of DOTAP, DPPC, cholesterol, DLin-MC3-DMA, and DSPE-PEG encapsulate mRNA for efficient delivery to alveolar epithelial cells (AECs) and fibroblasts in lungs undergoing fibrosis following intratracheal administration.

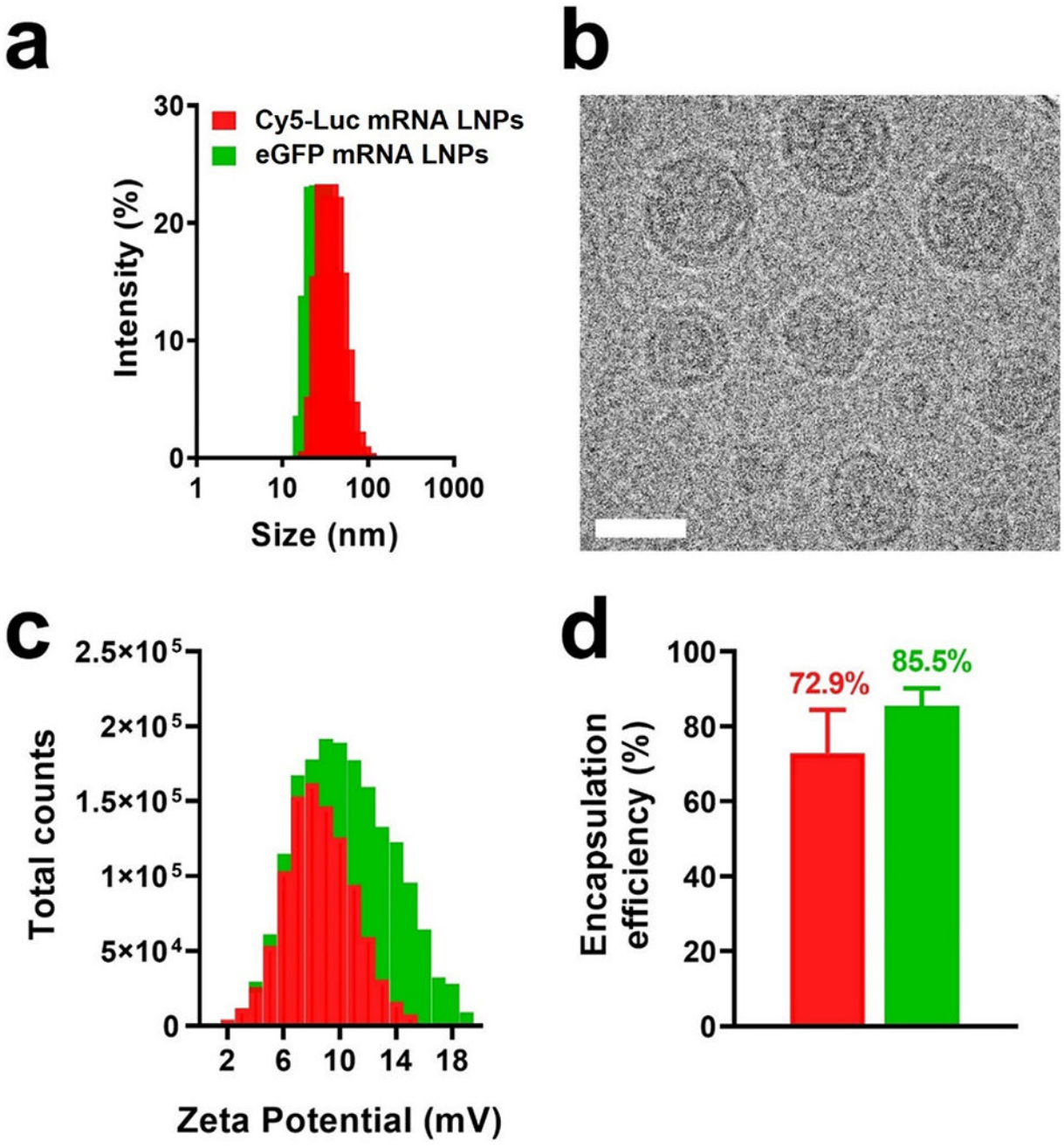

Fig. 2.

Physicochemical characterization and mRNA loading efficiency evaluation in LNPs. a) Diameter of mRNA-containing LNPs as determined via dynamic light scattering measurements. b) Cryo-TEM imaging of eGFP mRNA LNPs. The scale bar represents 25 nm. c) Surface charge of mRNA-containing LNPs as determined by zeta potential analysis. d) Loading efficiency of mRNA within LNPs. Results represent mean ± STDEV.

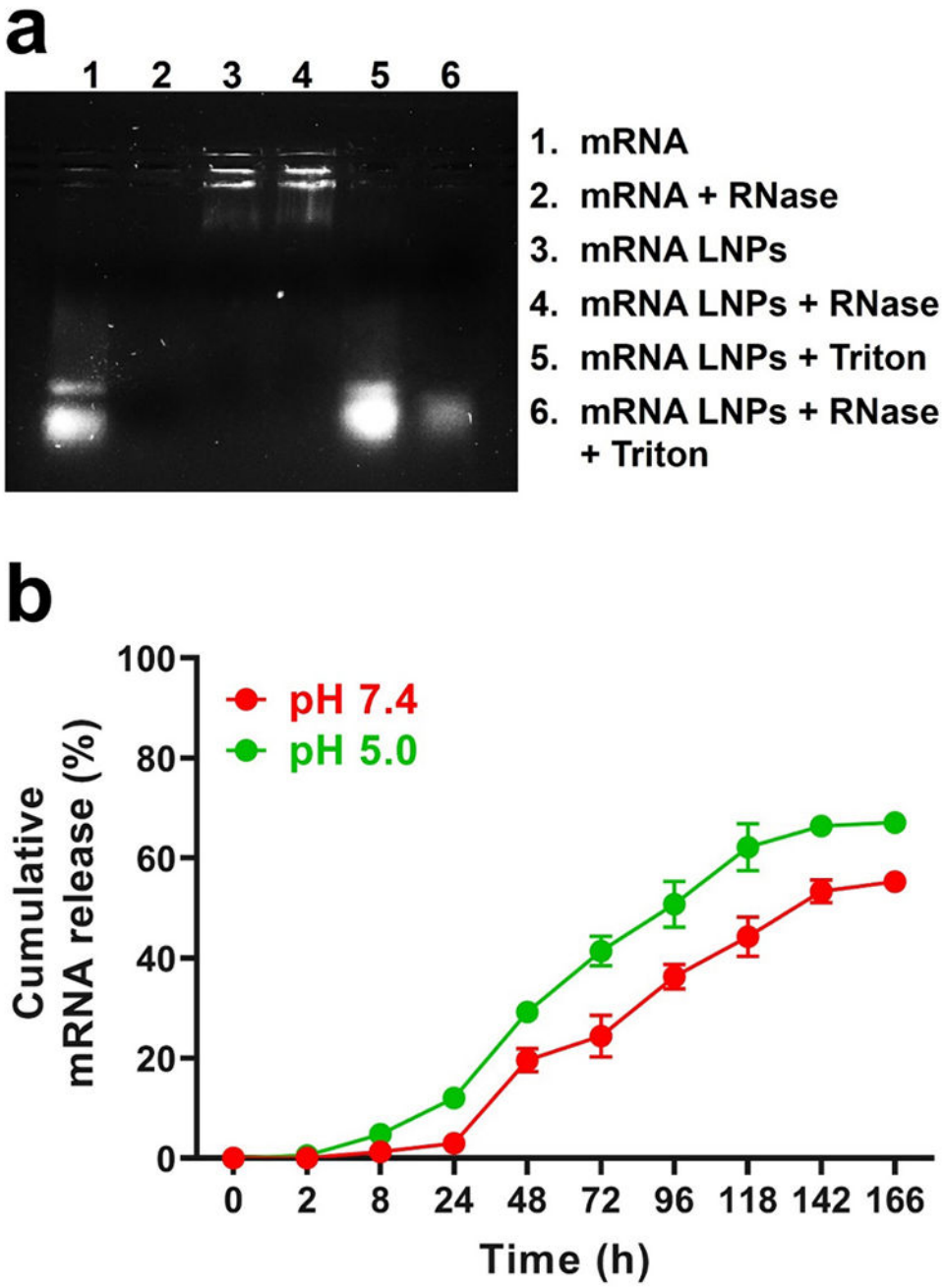

Fig. 3.

mRNA stability and release kinetics from LNPs. a) Gel retardation assay for encapsulated mRNA stability in the presence of RNase. b) *In vitro* cumulative release of mRNA release from LNPs in PBS at pH 5.0 and 7.4. Results represent mean ± STDEV.

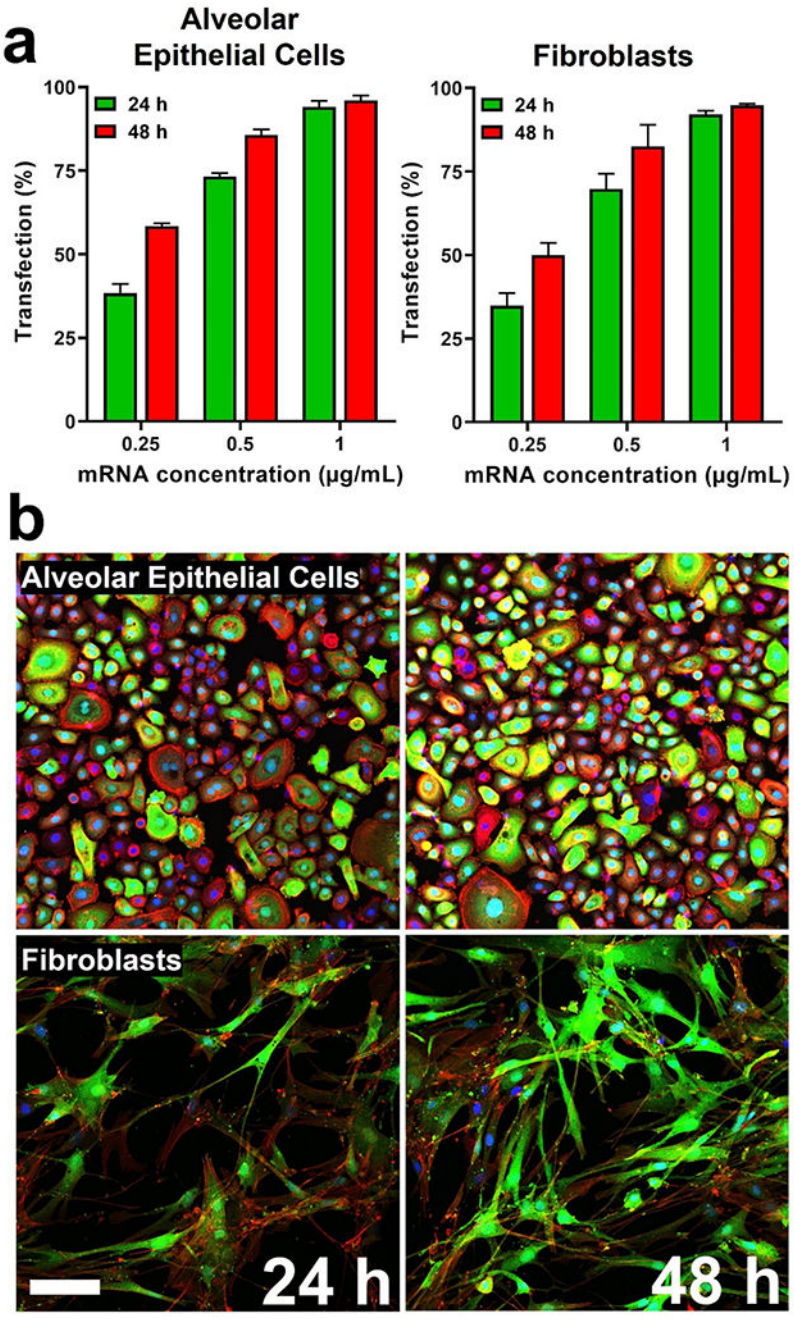

Fig. 4.

Transfection efficiency of eGFP mRNA LNPs in human primary alveolar epithelial cells and lung fibroblasts. a) mRNA transfection efficiency based on eGFP expression in alveolar epithelial cells and fibroblasts as determined by flow cytometry analysis. Results represent mean ± STDEV. b) Confocal microscopy examination of alveolar epithelial cells and fibroblasts at timepoints of 24 and 48 h after transfection with eGFP mRNA LNPs (1 μg/mL). eGFP is represented in green, while nuclei (DAPI) and F-actin appear as blue and red, respectively. The scale bar represents 25 μm.

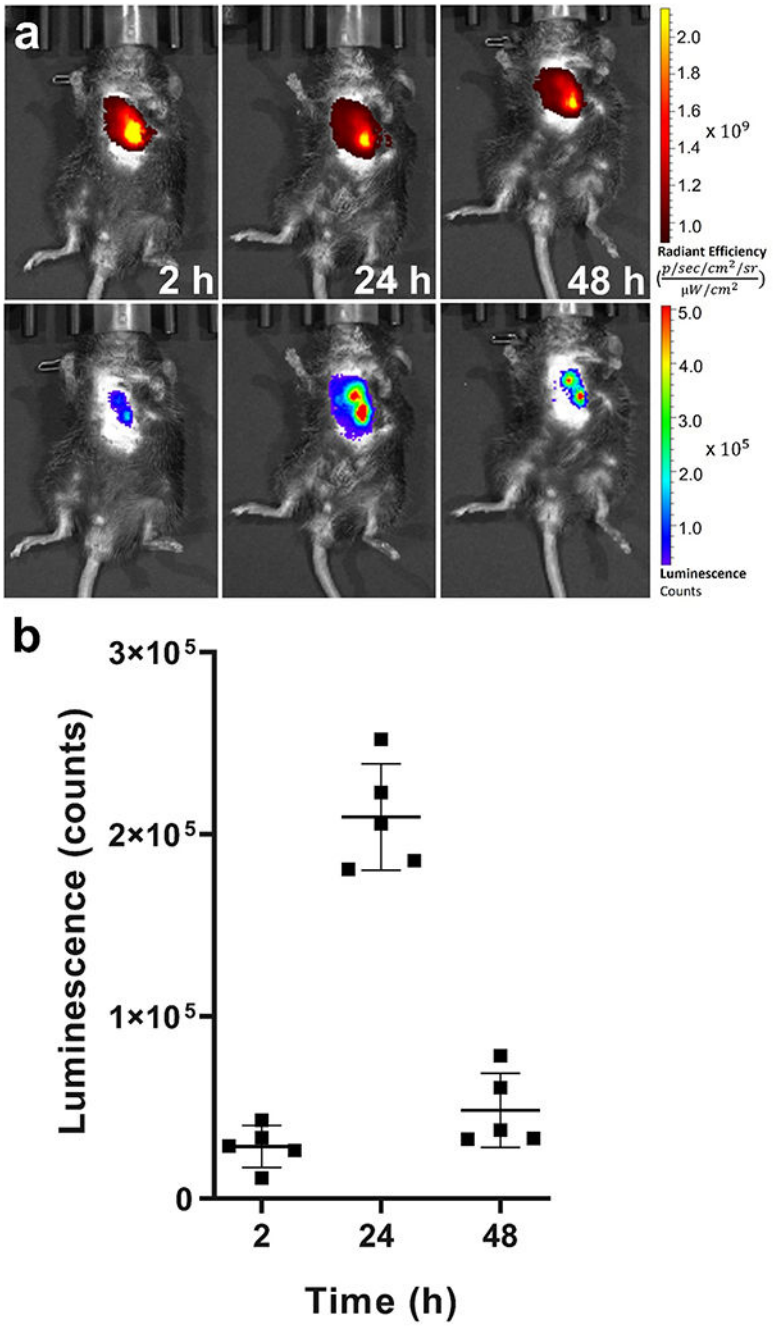

Fig. 5.

In vivo evaluation of luciferase expression following LNP delivery to lungs undergoing fibrosis. a) Representative whole-body bioluminescence images of bleomycin-treated mice at different timepoints after intratracheal administration of Cy5-Luc mRNA LNPs. Upper panel: Whole-body epifluorescence images. Lower panel: Corresponding bioluminescence after intraperitoneal injection of D-luciferin. b) Average radiance of luminescence in bleomycin-treated mice at different timepoints after intratracheal administration of Cy5-Luc mRNA LNPs (N=5). Results represent mean ± STDEV.

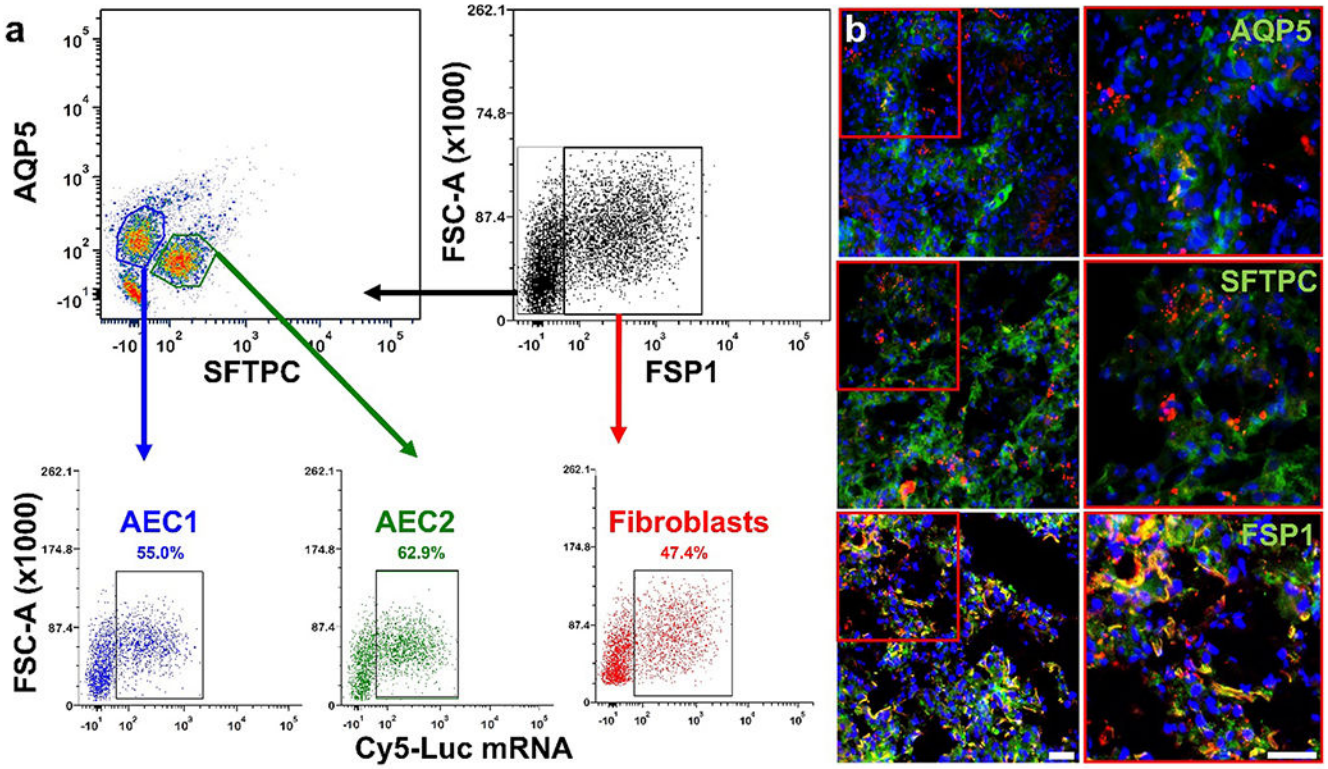

Fig. 6.

In vivo evaluation of LNP-delivered mRNA cell distribution in lungs undergoing fibrosis. Localization of Cy5-Luc mRNA in alveolar epithelial cells type 1 (AEC1) and 2 (AEC2), as well as fibroblasts, was examined in bleomycin-treated mouse lungs (N=3) 24 h after intratracheal administration of Cy5-Luc mRNA LNPs. a) Representative flow cytometry analysis of Cy5-Luc mRNA uptake in AEC1, AEC2, and lung fibroblasts. b) Representative confocal microscopy micrographs obtained from lung tissues. Red represents Cy5-Luc mRNA. The AEC1 marker AQP5, the AEC2 marker SFTPC, and the fibroblast marker FSP1 appear as green in the images, while DAPI (nuclear staining) appears as blue. The scale bars represent 50 μm.

Eur J Pharm Sci. Author manuscript; available in PMC 2024 February 27.

Table 1

Formulation parameters and physicochemical properties of eGFP mRNA LNPs.

Formulation	Composition		Size (nm)	Zeta potential (mV)	PDI	Encapsulation efficiency (%)	Cell viability (%)*
1	DOTAP	40%	102 ± 11.3	16.5 ± 3.2	0.37 ± 0.09	81.6 ± 4.9	87.6 ± 4.0
	DLin-MC3-DMA	20%					
	DPPC	10%					
	Cholesterol	28.50%					
	PEG-DSPE	1.50%					
2	DOTAP	40%	37.8 ± 6.4	47.9 ± 5.5	0.30 ± 0.07	85.6 ± 3.6	84.0 ± 3.5
	DLin-MC3-DMA	10%					
	DPPC	10%					
	Cholesterol	37%					
	PEG-DSPE	3%					
3	DOTAP	40%	122 ± 13.8	19.8 ± 3.6	0.39 ± 0.11	78.0 ± 6.6	89.0 ± 1.8
	DLin-MC3-DMA	10%					
	DPPC	10%					
	Cholesterol	28.50%					
	PEG-DSPE	1.50%					
4	DOTAP	50%	43.8 ± 8.6	27.4 ± 2.2	0.26 ± 0.7	87.0 ± 7.6	80.7 ± 1.8
	DLin-MC3-DMA	25%					
	DPPC	5%					
	Cholesterol	18.50%					
	PEG-DSPE	1.50%					
5	DOTAP	40%	34.2 ± 0.8	11.5 ± 2.4	0.29 ± 0.08	85.5 ± 5.3	83.8 ± 1.8
	DLin-MC3-DMA	25%					
	DPPC	10%					
	Cholesterol	23.50%					
	PEG-DSPE	1.50%					

*Viability derived from cell experiments at 1 μg/mL